

A LIGHT-CURVE MODEL OF THE SYMBIOTIC NOVA PU VUL (1979) – A VERY QUIET EXPLOSION WITH LONG-LASTED FLAT PEAK

MARIKO KATO

Department of Astronomy, Keio University, Hiyoshi, Yokohama 223-8521 Japan

IZUMI HACHISU

Department of Earth Science and Astronomy, College of Arts and Sciences, University of Tokyo, Komaba, Meguro-ku, Tokyo 153-8902, Japan

ANGELO CASSATELLA

INAF, Istituto di Fisica dello Spazio Interplanetario, Via del Fosso del Cavaliere 100, 00133 Roma, Italy
European Space Astronomy Center (ESAC), Villanueva de la Cañada, Apartado 78, 28691, Madrid, Spain and
Dipartimento di Fisica E. Amaldi, Università degli Studi Roma Tre, Via della Vasca Navale 84, 00146 Roma, Italy

AND

ROSARIO GONZÁLEZ-RIESTRA

XMM Science Operation Centre, ESAC, P.O. Box 78, 28091 Villanueva de la Cañada, Madrid, Spain
to appear in the Astrophysical Journal

ABSTRACT

We present a light curve model of the symbiotic nova PU Vul (Nova Vulpeculae 1979) that shows a long-lasting flat peak with no spectral indication of wind mass-loss before decline. Our quasi-evolution models consisting of a series of static solutions explain both the optical flat peak and ultraviolet (UV) light curve simultaneously. The white dwarf mass is estimated to be $\sim 0.6M_{\odot}$. We also provide a new determination of the reddening, $E(B - V) = 0.43 \pm 0.05$, from UV spectral analysis. Theoretical light curve fitting of UV 1455 Å provides the distance of $d = 3.8 \pm 0.7$ kpc.

Subject headings: binaries: symbiotic — nova, cataclysmic variables — stars: individual (PU Vul) — ultraviolet: stars — white dwarfs

1. INTRODUCTION

PU Vul was independently discovered by Y. Kuwano (Kozai 1979a) and M. Honda (Kozai 1979b) as a nova-like object. Subsequent observations revealed that PU Vul did not behave like a classical nova in its photometric and spectroscopic properties. After the rise to the optical maximum, PU Vul maintained an almost stable maximum of $V = 8.6$ from 1979 to 1987 except for a deep minimum in 1980. It started to fade in 1988 very slowly toward the pre-discovery magnitude of $B = 14.5 - 16.6$ (Liller & Liller 1979) and the photographic magnitude $m_{pg} = 15.0 - 16.5$ (Yamashita et al. 1982). Such a long-lasting flat peak and a very slow evolution of the light curve made this object quite different from ordinary novae. PU Vul was recognized to be a binary system consisting of an M giant and an outbursting component (Belyakina et al. 1982a; Friedjung et al. 1984) and also that the outburst is a thermonuclear runaway event on a white dwarf (WD) in a symbiotic binary (Kenyon 1986). There were debates on the origin of the deep minimum occurred in 1980 (see discussion in Kenyon 1986). After the second eclipse in 1994, it has been clear that PU Vul is an eclipsing binary with the orbital period of 13.4 yr. The observational properties are summarized in Table 1, that shows the discovery date, nova speed class, remarkable property of the light curve, indication of dust formation, observational evidence of eclipse, orbital period, peak magnitudes of m_V , information of UV 1455

Å continuum-band light-curve obtained from fitting of Model 1 (Section 4.1), i.e., peak value and full width of half maximum (FWHM), extinction in literature and our estimates, distance to PU Vul in literature and our estimates.

Spectral development of PU Vul was extensively studied by various authors (Yamashita et al. 1982, 1983; Iijima & Ortolani 1984; Belyakina et al. 1989; Goehermann 1991; Kanamitsu 1991a; Kanamitsu et al. 1991b; Tamura et al. 1992; Klein et al. 1994). The spectra mimicked those of an F supergiant (Yamashita et al. 1982; Kanamitsu 1991a) in the early phase and changed to A0 (Belyakina et al. 1989; Vogel & Nussbaumer 1992) from 1983 to 1986 as the excitation temperature gradually increased (Kanamitsu et al. 1991b). Yamashita et al. (1982) commented that the eruption must have been quite soft because no evidence of shell ejection, both in emission lines and shell absorption lines, was detected. The optical spectrum was strongly absorption-dominated until 1985 but changed to a distinct nebular spectrum in the second half of 1987 (Iijima 1989; Kanamitsu et al. 1991b). In 1990 the star had shown rich emission lines in the optical and UV spectrum, which are typical in the nebular phase and associated with an extended atmosphere of a WD (Vogel & Nussbaumer 1992; Kanamitsu et al. 1991b; Tomov et al 1991).

It is very interesting that there is no indication of strong winds in PU Vul in contrast to many other classical novae. Instead, optically thin mass-ejection

TABLE 1
OBSERVATIONAL PROPERTIES OF PU Vul

subject	data	units	comments
discovery date	... 5.82 April 1979	UT	Kozai (1979a)
nova speed class	... very slow		
light curve	... flat peak		
dust	... no		
eclipse	... yes		
orbital period	... 13.4	yr	
m_V of flat peak	... 8.6	mag	
peak of UV 1455 Å flux	... 6.0×10^{-13}	erg cm ⁻² s ⁻¹ Å ⁻¹	this work: Section 4
FWHM of UV 1455 Å	... 4.4	yr	this work: Section 4
$E(B - V)$... 0.29-0.5		see references ^a
$E(B - V)$... 0.43 ± 0.05		this work: Section 2.1
distance	... 1.6-7	kpc	see references ^b
distance	... 3.8 ± 0.7	kpc	this work: Section 4.4

^a $E(B - V) = 0.4$ (Belyakina et al. 1982b), 0.49 (Friedjung et al. 1984), 0.4–0.5 (Kenyon 1986), 0.50 (Goehermann 1991), 0.4 (Vogel & Nussbaumer 1992), 0.29 (Luna & Costa 2005)

^b $d = 5$ –7 kpc (Belyakina et al. 1982b), 5.3 kpc (Belyakina et al. 1984), < 5.6 kpc (Goehermann 1991), 1.6–2.0 kpc (Vogel & Nussbaumer 1992), 2.5 kpc (Hoard et al. 1996)

from WD photosphere was suggested from P Cygni line-profiles (Belyakina et al. 1989; Vogel & Nussbaumer 1992; Sion et al. 1993; Nussbaumer & Vogel 1996) or triple structure of IR emission lines (Bensammar et al. 1991). The line width corresponds to 1100–1200 km s⁻¹ in average full widths at zero intensity (Tomov et al 1991), ~ 2600 km s⁻¹ in Balmer emission wings (Iijima 1989), and 550–600 km s⁻¹ in UV spectra (Sion et al. 1993). Mass ejection was also suggested from X-ray emission detected with ROSAT on 10–12 November 1992 UT and interpreted as thermal bremsstrahlung with a temperature of 0.22 keV (2.6×10^6 K) (Hoard et al. 1996; Mürset et al. 1997). These authors suggested a collisional origin of the X-ray between a high-density, low-velocity cool wind from the M giant and a low-density, high-velocity hot wind from the WD in the context of common properties of symbiotic novae.

To summarize, the outburst of PU Vul was very quiet in the first ten years, and optically thin mass-ejection arises from 1988–1990 as the nova entered a coronal phase. These spectral features as well as the long-lasting flat peak make PU Vul quite different from many other classical novae in which optical magnitude decays quickly from its peak and spectrum indicates strong optically thick winds. This paper aims to model such a quite different evolution of PU Vul and to understand the cause of such properties.

Kato & Hachisu (2009) reexamined the conditions of occurrence of optically thick winds and found that optically thick winds occur in a limited range of the envelope (ignition) mass. For a relatively large envelope mass, optically thick winds are suppressed in a way that a large density-inversion layer appears and the gas-pressure gradient balances with the radiation-pressure gradient, the driving force of the winds. In massive WDs ($\gtrsim 0.7 M_\odot$), optically thick winds always occur, because the ignition mass of the wind-suppressed solutions are too massive to be realized in the actual novae. In less massive WDs ($\lesssim 0.5 M_\odot$), on the other hand, no winds are accelerated because the radiation-pressure gradient is too weak to drive the winds. In between them, i.e., $0.5 M_\odot \lesssim M_{\text{WD}} \lesssim 0.7 M_\odot$, both types of solutions (wind and wind-suppressed) can be realized depending

on the initial envelope mass. For a less massive envelope, optically thick winds are accelerated and a shell flash develops as a normal nova with strong winds. On the other hand, if the initial envelope mass is relatively large, optically thick winds are suppressed and a nova evolves without winds.

Kato & Hachisu (2009) also presented an idea that such wind-suppressed (no optically thick wind) evolution will be realized in a very slow nova that shows a long-lasting flat optical peak. If the optically thick wind occurs, as in many classical novae, the strong winds carry out most of the envelope matter in a short timescale, and the optical brightness quickly decays. Thus, the light curve has a sharp optical peak. On the other hand, in the wind-suppressed evolutions, the brightness decays very slowly, because the evolution timescale is determined only by hydrogen nuclear burning. Therefore, the nova stays at a low surface temperature for a long time, which makes a long-lasting flat optical peak. PU Vul is the first example of this new type of evolution.

In Section 2 we review observational results based on the *IUE* spectra. In Section 3 we briefly introduce our method and assumptions of the theoretical model. Section 4 shows how to estimate the WD mass from light curve fittings. Discussion and conclusions follow in Sections 5 and 6, respectively.

2. UV OBSERVATIONS

PU Vul had been monitored by *IUE* from February 1979 to September 1983 and from October 1987 to September 1996 at both low and high resolutions. A gallery of UV SWP spectra from 1992 to 1995 can be found in Nussbaumer & Vogel (1996).

In the following we revisit the problem of the color excess $E(B - V)$ of PU Vul, and describe the long term evolution of the emission lines. The evolution of the UV continuum will be described in Section 4.1. The ultraviolet spectra were retrieved from the *IUE* archive through the INES (*IUE* Newly Extracted Spectra) system¹, which also provides full details of the observations. The use of *IUE* INES data is particularly important for the determination of reddening correction because of the

¹ <http://sdc.laeff.inta.es/ines/>

implementation of upgraded spectral extraction and flux calibration procedures compared to previously published UV spectra.

2.1. Reddening Correction

Table 1 shows that the color excess $E(B - V)$ toward PU Vul in the literature lies in the range from 0.3 to 0.5. Given the large spread of these determinations, we have directly determined $E(B - V)$ from the strength of the 2200 Å feature seen in the UV spectra of PU Vul.

The Galactic extinction curve (Seaton 1979) shows a pronounced broad maximum around 2175 Å due to dust absorption. Since it takes the same value $X(\lambda) = A(\lambda)/E(B - V) \approx 8$ at $\lambda = 1512, 1878,$ and 2386 Å, the slope of the straight line passing through the continuum points at these wavelengths is insensitive to $E(B - V)$ in a $(\lambda, \log F(\lambda))$ plot. This circumstance can be used to get a reliable estimate of $E(B - V)$ as that in which the stellar continuum becomes closely linear in the 1512–2386 Å region, and passes through the continuum points at the above wavelengths. From 9 pairs of short and long wavelength *IUE* spectra taken from JD 2,448,217 to JD 2,450,342, i.e. during the nebular phase, we have in this way found $E(B - V) = 0.43 \pm 0.05$. Examples of *IUE* spectra of PU Vul corrected with $E(B - V) = 0.43$ are reported in Figure 1.

2.2. Evolution of the UV Continuum

We have measured the mean flux in two narrow bands 20 Å wide centered at 1455 Å and 2855 Å, selected to provide a fairly good representation of the UV continuum because little affected by emission lines (Cassatella et al. 2002). Figure 2 shows the time evolution of the $F(1455 \text{ Å})$ and $F(2855 \text{ Å})$ fluxes and of the UV color index $C(1455 - 2855) = -2.5 \log[F(1455 \text{ Å})/F(2855 \text{ Å})]$. The measurements were made on well exposed low resolution large aperture spectra. Figure 2 reports also, for comparison, the visual light curve obtained from the Fine Error Sensor (FES) counts, V_{FES} , on board *IUE*, once corrected for the time dependent sensitivity degradation (p.35 in Cassatella et al. 2004). Note the pronounced UV maximum around JD 2,447,400 followed by a progressive decay at the same time as the UV spectrum becomes harder, as indicated by the decrease of the UV color index. The delay of the UV maximum with respect to the visual maximum is common both to novae and symbiotic stars (Fernandez-Castro et al. 1995; Cassatella et al. 2002).

2.3. Evolution of the UV Emission Lines

Figure 3 reports, as a function of time, the observed fluxes in the emission lines of C III] 1909 Å, C IV 1550 Å, N IV] 1487 Å, He II 1640 Å, and N V 1240 Å, which cover a wide range of ionization conditions (the corresponding ionization energies χ_{ion} are 24.4, 47.9, 47.4, 54.4 and 77.5 eV, respectively). The flux measurements were obtained from well exposed *IUE* low resolution spectra. The figure shows clearly that the eclipse around JD 2,449,550 endures longer for high than for low ionization lines. This suggests that the high ionization lines are formed in the unseen side of the cool giant’s wind, so confirming the results by Nussbaumer & Vogel (1996) (see their Figure

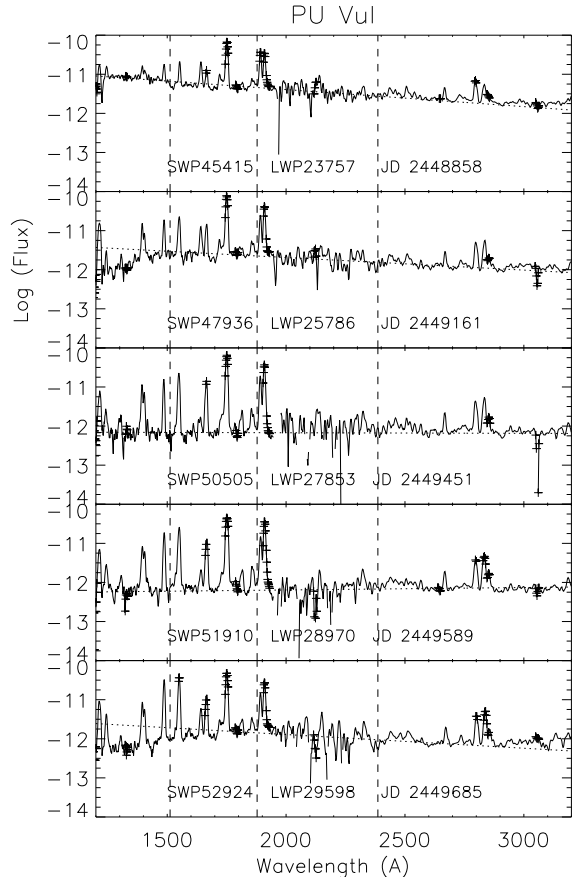


FIG. 1.— *IUE* spectra of PU Vul obtained at different dates. Fluxes are in units of $\text{erg cm}^{-2} \text{s}^{-1} \text{Å}^{-1}$. The spectra have been corrected for reddening using $E(B - V) = 0.43$. The vertical dotted lines represent the wavelengths $\lambda\lambda 1512, 1878$ and 2386 Å at which the extinction law takes the same value. With the adopted value of reddening, the stellar continuum underlying the many emission lines is well represented by a straight line all over the full spectral range. Saturated data points in the emission lines are labeled with pluses.

5), who found that the UV highest excitation lines of He II $\lambda 1640$, N V $\lambda 1240$, and N IV $\lambda 1718$ disappeared during the second eclipse.

3. MODEL

3.1. Evolution of Nova Outburst

Nova is a thermonuclear runaway event on a WD (Nariai et al. 1980; Prialnik 1986; Starrfield et al. 1972, 1988; José et al. 1998; Prialnik & Kovetz 1995). After unstable hydrogen nuclear burning triggers a nova outburst, the envelope on the WD greatly expands to a giant size. After it reaches the optical peak, the envelope expansion settles down into a steady-state. The optical magnitude decreases as the envelope mass decreases and the photospheric temperature rises with time. In less massive WDs the optically thick wind does not occur as described in Section 1 and, therefore, the decay phase of novae can be followed by a quasi-hydrostatic sequence (e.g., Iben 1982; Kato & Hachisu 1994, 2009). We solved the equations of hydrostatic balance, radiative diffusion, and conservation of energy from the bottom of the hydrogen-rich envelope through the photosphere. The bottom radius is assumed to be the Chandrasekhar

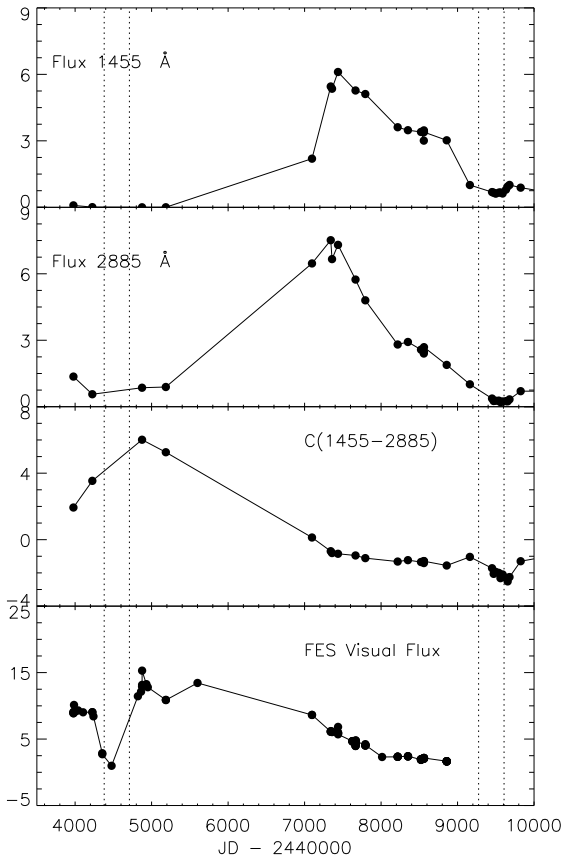


FIG. 2.— Evolution of the continuum fluxes at 1455 Å and 2885 Å, of the ultraviolet color index $C(1455 - 2885)$, and of the V_{FES} visual flux of PU Vul (see Section 2.2). Visual and UV fluxes are both in units of $10^{-13} \text{ erg cm}^{-2} \text{ s}^{-1} \text{ Å}^{-1}$, not corrected for reddening. Only the color index has been corrected for reddening using $E(B - V) = 0.43$ (see Section 2.1). The vertical dotted lines indicate the period of the first (JD 2,444,380 – 2,444,710) and the second (JD 2,449,275 – 2,449,608) eclipses.

radius. The evolution of novae is followed by connecting these solutions along the envelope mass-decreasing sequence. The time evolution is calculated from the mass decreasing rate which is the summation of the two rates, hydrogen nuclear burning and optically-thin wind mass-loss. We used OPAL opacities (Iglesias & Rogers 1996). The method and numerical techniques are essentially the same as those in Kato & Hachisu (1994). Convective energy transport is calculated using the mixing length theory with the mixing-length parameter $\alpha = 1.5$ (see Figure 11 in Kato & Hachisu 2009, for the dependence of model light curve on the mixing length parameter α).

In the rising phase, the envelope does not yet settle down to a thermal equilibrium, i.e., the nuclear energy generation is larger than the radiative loss. We have approximated such a stage by a sequence of static solutions of constant mass without thermal equilibrium. These solutions may not approximate well the rising phase, but are enough to our purpose, because the rising phase plays no important role in the determination of physical values such as the WD mass and distance.

3.2. Wind Mass-Loss Rate

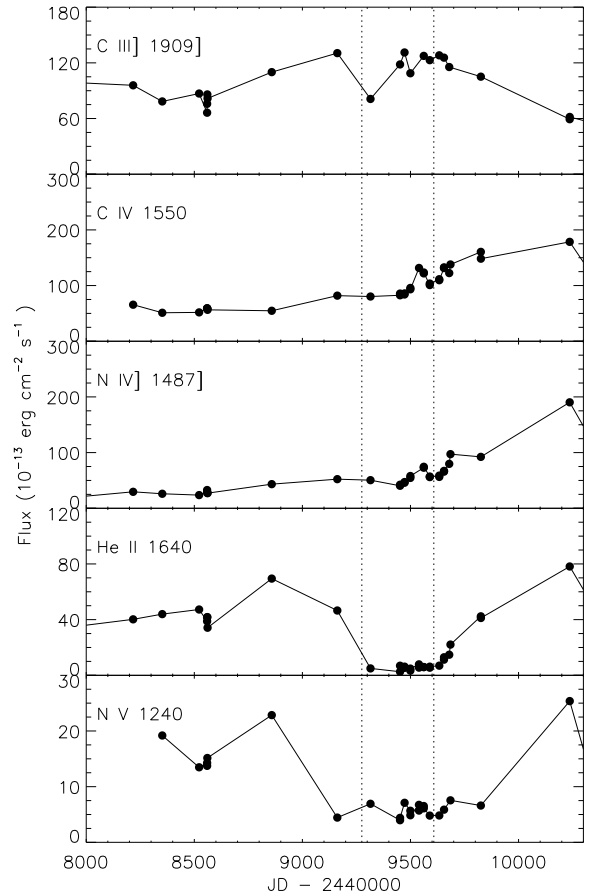


FIG. 3.— Observed fluxes of some prominent UV emission lines of PU Vul as a function of time. Fluxes are in units of $10^{-13} \text{ erg cm}^{-2} \text{ s}^{-1}$, not corrected for reddening.

In the later phase of the outburst (after 1986), optically-thin wind may arise because many emission lines had appeared in spectra. We cannot calculate such wind mass-loss, however, because radiative transfer in the optically-thin region is not included in our model calculation. Therefore, we take the wind mass-loss rate as a model parameter. This optically-thin wind does not affect the envelope structure below the photosphere, but speeds up the nova evolution because mass decreasing rate of the envelope is accelerated by this wind mass-loss.

In line driven winds, the mass-loss rate \dot{M} is limited by photon momentum; the wind cannot get momentum much exceeding the momentum of photon flux. This is in contrast to optically thick winds in which the mass-loss rate could be much larger than the momentum of photon flux (Kato & Iben 1992). Therefore, we assume a condition, that the momentum of wind is smaller than that of photon flux, of

$$\dot{M}v_{\text{wind}} < \frac{L_{\text{ph}}}{c}, \quad (1)$$

where c is the speed of light. We get an upper limit of the wind mass-loss rate as

$$\dot{M} < 1.6 \times 10^{-6} \left(\frac{L_{\text{ph}}}{6 \times 10^{37} \text{ erg s}^{-1}} \right) \left(\frac{v_{\text{wind}}}{200 \text{ km s}^{-1}} \right)^{-1} M_{\odot} \text{ yr}^{-1}. \quad (2)$$

Here we take $L_{\text{ph}} = 6 \times 10^{37} \text{ erg s}^{-1}$ from a bolometric luminosity of a $0.6 M_{\odot}$ WD (which will be shown later as Model 2 in Table 2), and assume a relatively small value of $v_{\text{wind}} = 200 \text{ km s}^{-1}$ for a safe upper limit.

Bensammar et al. (1991) estimated the mass-loss rate of PU Vul to be about $4 \times 10^{-6} M_{\odot} \text{ yr}^{-1}$ from emission measure on 30 April and 1 May 1988 with a wind velocity of 70 km s^{-1} and a hot star radius of $3.9 \times 10^{12} \text{ cm}$ ($56 R_{\odot}$). Sion et al. (1993) set an upper limit of the mass-loss rate, $1 \times 10^{-5} M_{\odot} \text{ yr}^{-1}$. Skopal (2006) estimated the mass-loss rate from $H\alpha$ line luminosity of $144 L_{\odot}$ on 28 September 1988, assuming optically-thin fully-ionized winds. With a terminal velocity $2,100 \text{ km s}^{-1}$ of a given velocity profile, Skopal obtained the mass-loss rate to be $\dot{M} = 5 \times 10^{-6} M_{\odot} \text{ yr}^{-1}$. These values, however, may be a little bit larger than our momentum condition (1).

In our model, we assume no wind mass-loss during the optical flat peak because no emission lines are observed or they are very weak. We assume that optically thin-wind begins when the photospheric temperature rises to $\log T_{\text{ph}} \text{ (K)} \sim 4.0$. This wind seems to have much weakened sometime around 1999-2001, because, after that, the optical light curve changed its shape and seems to decay as t^{-3} , where t is the time after the decay started. In classical novae, the t^{-3} decay is often observed in the later phase of the outburst, and is interpreted as emission from homologously expanding optically thin plasma with a constant mass, which indicates that the mass supply had stopped (Hachisu & Kato 2006, 2010). In the case of PU Vul, the wind had not stopped entirely since P Cyg profiles are still observed in 2004 (Yoo 2007). Therefore, we assume that the optically-thin wind begins at $\log T_{\text{ph}} \text{ (K)} = 4.0$ and continues until $\log T_{\text{ph}} \text{ (K)} = 5.05$ at a rate shown later, and after that the wind mass-loss rate dropped to $\dot{M} = 1.0 \times 10^{-7} M_{\odot} \text{ yr}^{-1}$.

3.3. Multiwavelength Light Curves

After the maximum expansion of the photosphere, the photospheric radius (R_{ph}) gradually decreases keeping the total luminosity (L_{ph}) almost constant. The photospheric temperature (T_{ph}) increases with time because of $L_{\text{ph}} = 4\pi R_{\text{ph}}^2 \sigma T_{\text{ph}}^4$. The maximum emission shifts from optical to supersoft X-ray through ultraviolet (UV). This causes the luminosity decrease in optical and increase in UV and finally increase of supersoft X-ray. We assume that photons are emitted at the photosphere as a blackbody with a photospheric temperature T_{ph} . The light curve of optical (V) and UV 1455Å fluxes are estimated from the blackbody emission.

3.4. Chemical Composition

Belyakina et al. (1989) obtained chemical composition of the atmosphere of the hot component of PU Vul, in which iron is depleted by a factor of 0.3–0.5 against the sun. The number ratio of He/H is estimated to be 0.31 (Andrillat & Houziaux 1994) and 0.146 (Luna & Costa

2005) from emission line ratios, which shows helium overabundance than the solar value (He/H ~ 0.08). Another suggestion comes from the location in the Galaxy. Belyakina et al. (1982b) suggested that PU Vul does not belong to the planar component of the Galaxy because the star is off the galactic plane by 0.7–1.0 kpc, based on their derived distance of 5–7 kpc. This value, however, reduced to 0.5 kpc if we adopt the distance of ~ 3.8 kpc as we will obtain later.

With the information above we assume the mass fraction of hydrogen, helium and heavy elements of the envelope to be $(X, Y, Z) = (0.5, 0.494, 0.006)$. For comparison, we further assume additional sets of composition i.e., $(0.5, 0.49, 0.01)$, $(0.7, 0.28, 0.02)$ and $(0.7, 0.29, 0.01)$. We simply assumed that the chemical composition of the envelope is uniform and constant with time.

4. LIGHT CURVE FITTING

4.1. UV Light Curve Fitting and the WD mass

The UV 1455 Å flux provides a good representation of the continuum level in novae, because it coincides with a local minimum of line opacity (Cassatella et al. 2002). In previous papers (Hachisu & Kato 2006; Hachisu et al. 2008; Kato et al. 2009), we have shown that the UV 1455 Å continuum light curve is very sensitive to model parameters, especially the WD mass.

Figure 4 shows time evolution of the UV 1455 Å continuum flux as well as our theoretical light curves. Figure 4a shows dependence on the WD mass for a given set of the wind mass-loss rate of $1 \times 10^{-7} M_{\odot} \text{ yr}^{-1}$ (arbitrarily chosen but not too small compared with the nuclear burning rate of $3 \times 10^{-7} M_{\odot} \text{ yr}^{-1}$) and chemical composition of $X = 0.5$ and $Z = 0.006$. We see that the UV peak is narrower in more massive WDs, because nova evolves faster owing to a less massive envelope and a high nuclear burning rate. Figure 4b depicts four light curves with different wind mass-loss rates for a given WD mass and chemical composition. As the assumed wind mass-loss rate is comparable to the nuclear burning rate ($3 \times 10^{-7} M_{\odot} \text{ yr}^{-1}$), the evolution speed of nova is sensitive to the mass-loss rate. Figure 4c shows five light curves with different sets of chemical composition. Nova evolves faster for smaller X , because of less nuclear fuel, and also faster for larger Z because of a smaller envelope mass.

In this way we can choose a WD mass with reasonable agreement with the UV data for a given parameter set of the wind mass-loss rate and composition, $(X, Y, Z) = (0.5, 0.494, 0.006)$. Table 2 shows two such models, one is a $0.57 M_{\odot}$ WD with the wind mass-loss rate of $5 \times 10^{-7} M_{\odot} \text{ yr}^{-1}$ (Model 1) and the other is a $0.6 M_{\odot}$ WD with $3 \times 10^{-7} M_{\odot} \text{ yr}^{-1}$ (Model 2). These WD masses, $0.57 M_{\odot}$ and $0.6 M_{\odot}$, are not much different, because they are in the middle of the permitted range of the WD mass, 0.53 – $0.65 M_{\odot}$, as explained below to avoid extremely small and large mass-loss rates. The 0.57 and $0.6 M_{\odot}$ models correspond respectively to the left and upper sides to the “wind region” (a triangle region in Figure 10 of Kato & Hachisu 2009) for the corresponding composition.

During the outburst, the photospheric temperature gradually rises and the photospheric radius decreases, with an almost constant photospheric luminosity. Figure

TABLE 2
SUMMARY OF OUR MODELS

subject	model 1	model 2	units
X	...	0.5	
Y	...	0.494	
Z	...	0.006	
WD mass	...	0.57	M_{\odot}
distance from UV fit ^a	...	3.7	kpc
$M_{V,\text{peak}}$ ^b	...	-5.49	mag
L_{peak} ^b	...	5.2	$10^{37} \text{erg s}^{-1}$
H-burning rate ^c	...	2.7	$10^{-7} M_{\odot} \text{yr}^{-1}$
maximum radius	...	62	R_{\odot}
initial envelope mass ^d	...	5.8	$10^{-5} M_{\odot}$
assumed wind mass-loss rate ($T < 5$) ^e	...	5.0	$10^{-7} M_{\odot} \text{yr}^{-1}$
assumed wind mass-loss rate ($T > 5$) ^f	...	1.0	$10^{-7} M_{\odot} \text{yr}^{-1}$
mass lost by the wind ($T < 5$) ^e	...	0.60	$10^{-5} M_{\odot}$
mass lost by the wind ($T > 5$) ^f	...	0.61	$10^{-5} M_{\odot}$

^a with $E(B - V) = 0.43$

^b values at $\log T_{\text{ph}}(\text{K})=3.9$

^c values at $\log T_{\text{ph}}(\text{K})=4.5$

^d the mass at the rising phase.

^e optically-thin wind from $\log T_{\text{ph}}(\text{K}) = 4$ to 5.05.

^f optically-thin wind at $\log T_{\text{ph}}(\text{K}) > 5.05$

5 shows the developments of the temperature and radius of Model 1 and Model 2 as well as observational estimates taken from literature. Vogel & Nussbaumer (1992) suggested that the temperature was as low as 6,000 K in 1979 as an effective temperature of F-supergiant and estimated the temperature to be 40,000 K $< T < 50,000$ K at 1991 from nebular spectra. They also obtained the radius of $\sim 50R_{\odot}$ from the analysis of 1980 eclipse. Kenyon (1986), Belyakina et al. (1989), and Gochermann (1991) estimated the temperature from spectral type. These values are plotted in Figure 5, in which our model temperature well reproduces observational estimates including the epoch around the UV1455 Å light curve peak, i.e., JD 2,447,000 to 2,448,200. The model radius is also consistent with observations considering large ambiguity in the estimating methods.

Table 3 shows the upper and lower limits of the WD mass that reproduces reasonable fitting to the UV light curve. For a given chemical composition, the maximum WD mass is obtained with no wind mass-loss, because more massive WDs produce much narrower UV curves. A more massive WD than the maximum value in Table 3 produces a UV light curve too narrow to fit the observation. On the other hand, for less massive WDs, we need to assume larger wind mass-loss rates because of their slower evolutions. The minimum WD mass may be obtained for a largest wind mass-loss rate that we adopt $1 \times 10^{-6} M_{\odot} \text{yr}^{-1}$ from Equation (2). With plausible values of the optically thin wind-mass-loss rate, which may be a few to several $\times 10^{-7} M_{\odot} \text{yr}^{-1}$, we may conclude that the WD is about $0.6M_{\odot}$.

4.2. Optical Light Curve

Figure 6 shows optical light curves of Model 1 and Model 2, of which characteristic values are summarized in Table 2. These two models are selected from fitting with the UV light curves, but also well reproduce the optical light curve in the flat maximum as well as the following decline until 1989, except the first eclipse in 1980 which is not taken into account in our model.

After 1989 the theoretical light curve largely deviates

from observed optical magnitudes. In this stage, spectra are emission-line dominated and the continuum is very weak (Yoo 2007). These emission lines comes from optically thin plasma outside the photosphere which is not included in our model. Therefore, our theoretical models give much lower magnitudes than that of observational data.

In our theoretical models, the flat peak corresponds to the era of low photospheric temperature (7,000–9,000 K) as shown in Figure 5. The temperature gradually rises with time and reaches 10,000 K which is indicated by the cross in Figure 6, where we assume the optically-thin mass-loss begins. After that the nova entered the coronal phase and many emission lines appeared (Kanamitsu et al. 1991b; Nussbaumer & Vogel 1996). Our model temperature is consistent with these observational properties.

4.3. Internal Structure of the Envelope at the Flat Peak

Figure 7 shows internal structures of the envelopes of Model 1 and Model 2 with the photospheric temperature $\log T_{\text{ph}}(\text{K}) \sim 3.9$. Here, the local Eddington luminosity is defined as

$$L_{\text{Edd}} \equiv \frac{4\pi cGM_{\text{WD}}}{\kappa}, \quad (3)$$

where κ is the opacity in which we use the OPAL opacity. Since the opacity κ is a function of temperature and density, the Eddington luminosity is also a local variable. This Eddington luminosity has the deepest local minimum at $\log \bar{R}(\text{cm}) = 10.4 - 11.2$ that corresponds to the Fe peak of OPAL opacity. There appears a large density-inversion layer at $\log r(\text{cm}) \sim 10.2 - 11.2$ corresponding to the super Eddington region ($L_{\text{Edd}} < L_r$). This density-inversion arises in order to keep hydrostatic balance in the super-Eddington region. Such a structure is very different from ordinary nova wind solutions, in which the density monotonically decreases as r^{-2} (Kato & Hachisu 1994, 2009), but similar to that of red giants.

TABLE 3
UPPER AND LOWER VALUES OF THE WD MASS

composition	minimum mass ^a	maximum mass ^b
$X = 0.5, Y = 0.294, Z = 0.006$...	$0.53 M_{\odot}$	$0.65 M_{\odot}$
$X = 0.5, Y = 0.29, Z = 0.01$...	$0.5 M_{\odot}$	$0.62 M_{\odot}$
$X = 0.7, Y = 0.28, Z = 0.02$...	$0.5 M_{\odot}$	$0.67 M_{\odot}$
$X = 0.7, Y = 0.29, Z = 0.01$...	$0.52 M_{\odot}$	$0.72 M_{\odot}$

^a in case of a very large mass-loss rate of $1 \times 10^{-6} M_{\odot} \text{ yr}^{-1}$

^b extreme case of no wind mass-loss

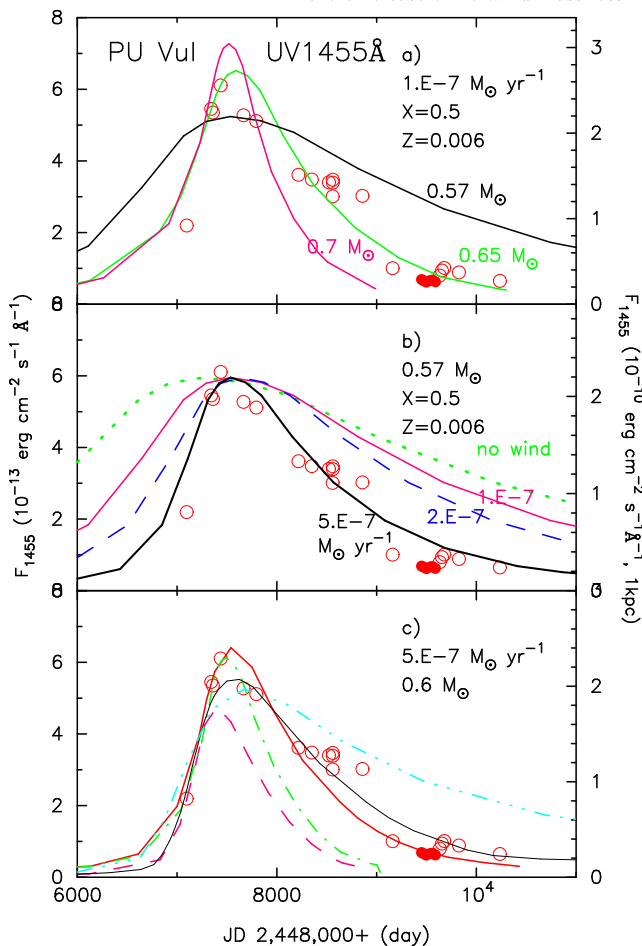


FIG. 4.— UV 1455 Å light curves. The UV 1455 Å data are denoted by red open circles (outside the eclipse) and red filled circles (during the eclipse). Theoretical UV light curves are shown in curves for an assumed distance of 1 kpc (with right-side axis). a) Comparison among different WD masses for the same wind mass-loss rate ($1 \times 10^{-7} M_{\odot} \text{ yr}^{-1}$) and the same chemical composition of $X = 0.5$ and $Z = 0.006$. The WD mass is indicated beside each line. b) Comparison among different mass-loss rates for the $0.57 M_{\odot}$ WD with composition of $X = 0.5$ and $Z = 0.006$. The wind mass-loss rate (in units of $M_{\odot} \text{ yr}^{-1}$) is attached to each curve. c) Comparison among different chemical compositions for the same mass-loss rate of $5 \times 10^{-7} M_{\odot} \text{ yr}^{-1}$ and WD mass of $0.6 M_{\odot}$. The chemical composition is $(X, Z) = (0.7, 0.004)$ for a three-dot-dashed curve, $(0.5, 0.006)$ for a thick solid curve, $(0.7, 0.01)$ for a thin solid curve, $(0.5, 0.01)$ for a dash-dotted curve, and $(0.7, 0.02)$ for a dashed curve.

These two solutions are representative of those in the long-lasting flat-peak in the optical light curve (Figure 6), i.e., the envelope is extended to $50\text{--}60 R_{\odot}$ and the temperature is as low as $\log T_{\text{ph}} \text{ (K)} \sim 3.9\text{--}4.0$. The convection, which is dominant in energy transport in the rising

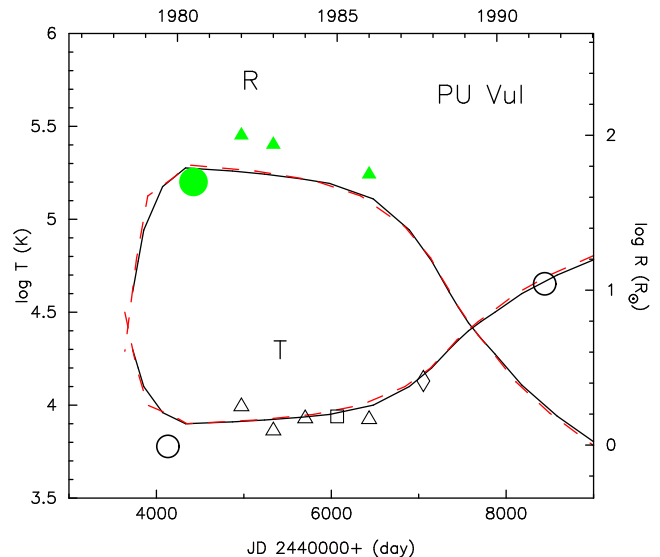


FIG. 5.— Development of the temperature and radius of the hot component (WD photosphere) in PU Vul. Curves denote the blackbody temperature and the photospheric radius of our Model 1 (Solid line) and Model 2 (Dashed line). The effective temperature (open symbols) and radius (filled symbols) estimated by various authors are also shown. Circles: Vogel & Nussbaumer (1992). Triangles: Belyakina et al. (1989). Diamonds: Goehermann (1991). Square: Kenyon (1986).

phase of nova outbursts (Priyalnik 1986), has retreated and is ineffective in and after the flat-peak. The convection occurs where the opacity decreases outward, i.e., the local Eddington luminosity increases outward. The largest convective region is at $\log r \text{ (cm)} = 10.5\text{--}11.4$, corresponding to the super-Eddington region (see Figure 7). In all convective regions, convection is ineffective in energy transport due to low density, and unable to carry all of the energy flux. Therefore, the structure is super-adiabatic, i.e., entropy decreases outward. This situation is different from the convective core of intermediate-mass main-sequence star or the inner convective envelope of low-mass red giant star, where the convective energy transport is effective and the temperature gradient is very close to the adiabatic gradient (Hayashi et al. 1962; Iben 1965).

The Eddington luminosity with electron scattering opacity $L_{\text{Edd,el}} = 4\pi cGM/[0.2(1+X)]$ is often used as an easy estimate of the WD luminosity. We note, however, that the photospheric luminosity is only 54 % of $L_{\text{Edd,el}}$ for Model 1 ($0.57 M_{\odot}$ WD) and 57 % for Model 2 ($0.6 M_{\odot}$ WD).

4.4. Distance

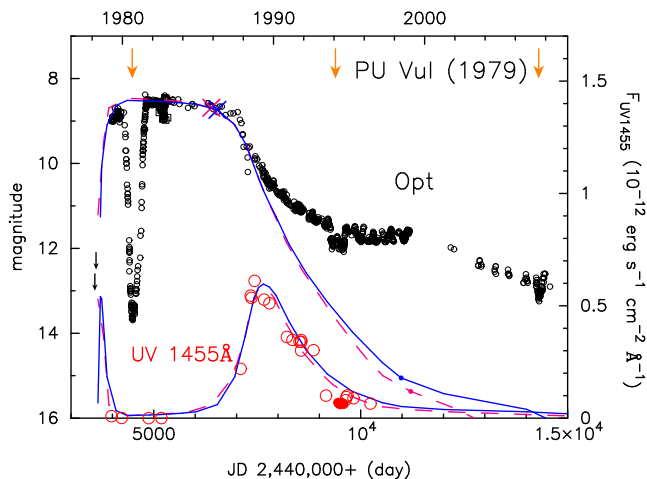


FIG. 6.— Optical and UV light curves of PU Vul. Optical data are taken from IAU Circular (for dip: 3421, 3477, 3494, 3589, 3604, 3610, and 3655), Wenzel (1979), Yamashita et al. (1982), Belyakina et al. (1982b), Chochol, Hric, & Papousek (1981), Purgathofer & Schnell (1982), Kolotilov (1983), Purgathofer & Schnell (1983), Iijima & Ortolani (1984), Iijima (1989), Kanamitsu et al. (1991b), Klein et al. (1994), Kolotilov et al. (1995), Yoon & Honeycutt (2000), and AAVSO (after JD 2,452,000). Large red open circles denote the flux of *IUE* UV 1455 Å band. Calculated light curves are also shown for Model 1 (Thin solid line) and Model 2 (Dashed line). The scale in the right-hand-side axis denotes that for observational data. Scale for the theoretical UV flux is (bottom, top)=(0, 6.25) for Model 1 and (0, 7.0) for Model 2 in units of $10^{-6} \text{ erg s}^{-1} \text{ cm}^{-2} \text{ \AA}^{-1}$ for the distance of 10 pc. The cross/small dot indicate starting/end point of the assumed optically-thin wind mass-loss. See text for more details.

The distance to PU Vul is obtained from the comparison of the 1455 Å band flux with the corresponding model fluxes (Hachisu & Kato 2006; Kato & Hachisu 2005, 2007). The flux of Model 1 is $F_{\lambda}^{\text{mod}} = 2.2 \times 10^{-6} (d/10 \text{ pc})^2 \text{ ergs cm}^{-2} \text{ s}^{-1} \text{ \AA}^{-1}$ at the peak. The corresponding observed flux is $F_{\lambda}^{\text{obs}} = 6.0 \times 10^{-13} \text{ ergs cm}^{-2} \text{ s}^{-1} \text{ \AA}^{-1}$ as in Figure 6. From these values we obtain the distance of $d = 3.7 \text{ kpc}$ with the absorption $A_{\lambda} = 8.3 \times E(B - V)$ for $\lambda = 1455 \text{ \AA}$ (Seaton 1979), here we use $E(B - V) = 0.43$ (obtained in Section 2.1). If we use the upper and lower limit of $E(B - V) = 0.43 \pm 0.05$, we get the distance of $d = 3.7_{-0.6}^{+0.7} \text{ kpc}$. The error coming from the UV flux fitting is much smaller and up to $\pm 0.15 \text{ kpc}$. In the same way, we obtain $d = 3.9_{-0.6}^{+0.7}$ for Model 2. If we adopt a different set of chemical composition, the resultant distance is also changed. For the $0.6 M_{\odot}$ WD we obtain 3.8 kpc for $(X, Z) = (0.5, 0.01)$, 3.3 kpc for $(0.7, 0.02)$ and 3.5 kpc for $(0.7, 0.01)$. Taking into account that $Z = 0.02$ is a bit larger than the recent estimate of solar value ($Z = 0.0128$; Grevesse 2008), 3.3 kpc may be a smaller limit. Thus, we may summarize our distance estimates as $d = 3.8 \pm 0.7 \text{ kpc}$. The error includes ambiguity of the $E(B - V)$, WD mass, and chemical composition.

5. DISCUSSION

As described in Section 3, a nova becomes a supersoft X-ray source in the later phase of the outburst. In PU Vul, however, the maximum temperature is not high enough compared with a typical classical nova because of the less massive WD ($\sim 0.6 M_{\odot}$). Our theoretical model predicts that the outburst of PU Vul is still ongoing and

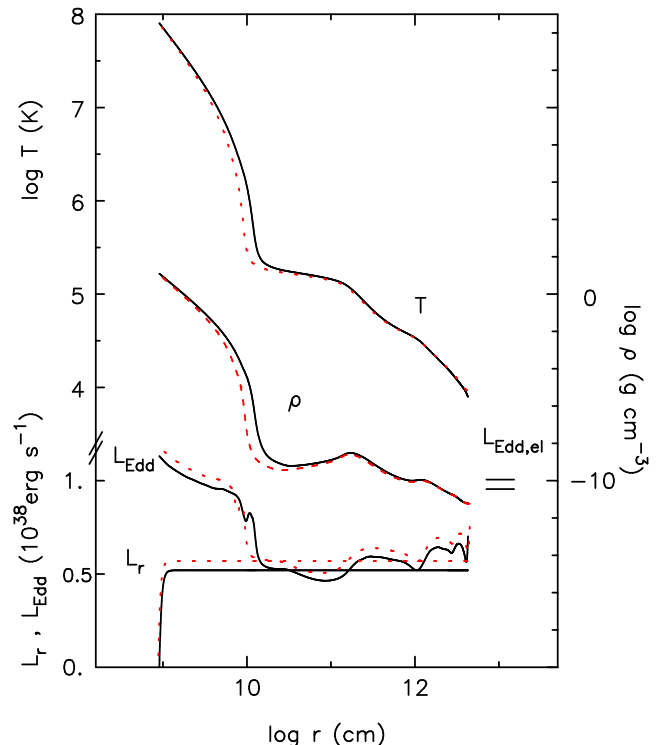


FIG. 7.— Temperature (T), density (ρ), diffusive luminosity (L_r), and the local Eddington luminosity (L_{Edd}) of envelope solutions at $\log T_{\text{ph}} = 3.9$ for Model 1 (solid curve) and Model 2 (dotted curve). The right edge of the curve corresponds to the photosphere and the left edge to the bottom of the envelope, i.e., bottom of the nuclear burning region. Two short horizontal lines indicate Eddington luminosity with electron scattering opacity, $L_{\text{Edd,el}} = 4\pi cGM/[0.2(1+X)]$ for Model 1 (lower line) and Model 2 (upper line).

the temperature is continuously rising. The temperature will finally reach the maximum temperature of $\sim 3 \times 10^5 \text{ K}$ just before hydrogen burning stops (X-ray turnoff), while the flux is almost constant at $2 - 3 \times 10^{37} \text{ erg s}^{-1}$. Therefore, we may expect supersoft X-ray from PU Vul in future, but it is very difficult to predict this epoch, because it strongly depends on the model parameters, such as the optically-thin wind mass-loss rate, and the chemical composition of the envelope.

No X-ray observations of PU Vul have been made since November 1992. The detected X-ray flux was attributed to a shock origin of colliding winds (Hoard et al. 1996; Mürset et al. 1997). PU Vul is a symbiotic nova in which the M-giant companion blows a massive cool wind that may preferentially distribute in the orbital plane. This cool wind may prevent a clear detection of supersoft X-rays from the hot WD. Therefore, the probability of detecting supersoft X-rays would be higher when the WD is in front of the cool wind of the giant (around 2014) and would be very low near the eclipse (2020-2021).

We have performed simulations for detectability of supersoft X-ray with the assumed values of $E(B - V) = 0.43$ and $d = 3.8 \text{ kpc}$. It will be possible to detect PU Vul at 0.007 cts s^{-1} with the EPIC-pn camera onboard *XMM-Newton* when the temperature is $\log T (\text{K}) \sim 5.3$ and the luminosity is $\sim 5 \times 10^{37} \text{ erg s}^{-1}$ (probably in 2010-2020) and at about 1 cts s^{-1} near the X-ray turnoff time, i.e., $\log T (\text{K}) \sim 5.5$ and $\sim 2 \times 10^{37} \text{ erg s}^{-1}$ (prob-

ably in 2060–2090). However, these estimates are based on our Model 1 and Model 2 only, and there is a large ambiguity due to uncertainty of the model parameters and assumptions. Especially the above expecting year depends strongly on the assumed wind-mass-loss rate after the photospheric temperature of the WD envelope rises to $\log T$ (K) = 5.05. If the wind-mass-loss will much weaken, the X-ray turnoff time is much later than the above estimates.

We expect that a large part of the envelope will remain on the WD after the outburst of PU Vul, because no optically thick wind occurs. From the initial envelope mass and the matter lost by the optically-thin wind as in Table 2, we estimate the envelope mass that will remain after the outburst. Highly depending on the assumed mass-loss rate as well as the other parameters, it is estimated to be about 70–90 % of the initial envelope mass for reliable model parameters. Mass-accreting WDs are, in general, potential candidates of progenitors of Type Ia supernovae (SNe Ia). However, low mass WDs ($\lesssim 0.9M_{\odot}$) such as in PU Vul have not been considered as a candidate of SNe Ia, because it is hard to grow to Chandrasekhar mass limit (e.g. Hachisu et al. 1999a,b; Kato 2010).

6. CONCLUSIONS

Our main results are summarized as follows:

1. Based on the idea of Kato & Hachisu (2009) that a

long-lasting flat peak of optical light curves can be reproduced by a sequence of wind-suppressed static-solutions, we have succeeded in reproducing the long-lasting optical flat peak of PU Vul as well as the UV 1455 Å continuum light curve. Our model is consistent with spectral features with no indication of strong winds in the flat peak of PU Vul.

2. An analysis of the *IUE* spectra of PU Vul indicates $E(B - V) = 0.43 \pm 0.05$.

3. We obtain a mass range of the WD between 0.55 and 0.65 M_{\odot} by comparing our theoretical light curves with the UV light curve.

4. We obtain the distance of $d = 3.8 \pm 0.7$ kpc with $E(B - V) = 0.43 \pm 0.05$.

5. We may conclude that the outburst of PU Vul is still on-going, and has already entered the supersoft X-ray phase. We encourage X-ray observations in ~ 2014 , when the WD is in front of the red giant, that will provide important information on this symbiotic nova.

We would like to thank Joanna Mikołajewska for valuable discussion on observational features of PU Vul. We are also grateful to the anonymous referee for useful comments that helped to improve the manuscript. We also thank the American Association of Variable Star Observers (AAVSO) for the visual data of PU Vul. This research has been supported in part by the Grant-in-Aid for Scientific Research (20540227,22540254) of the Japan Society for the Promotion of Science.

REFERENCES

- Andrillat, Y., & Houziaux, L. 1994, *MNRAS*, 271, 875
 Belyakina, T.S., Gershberg, R.E., Efimov, Yu.S., Krasnobabtsev, V.I., Pavlenko, E.P., Petrov, P.P., Chuvavaev, K.K., & Shenavrin, V.I. 1982, *Sov. Astron.* 26, 2
 Belyakina, T.S., Gershberg, R.E., Efimov, Yu.S., Krasnobabtsev, V.I., Pavlenko, E.P., Petrov, P.P., Chuvavaev, K.K., & Shenavrin, V.I. 1982, *Sov. Astron.* 26, 184
 Belyakina, T.S. et al. 1984, *A&A*, 132, L12
 Belyakina, T.S. et al. 1989, *A&A*, 223, 119
 Bensammar, S., Friedjung, M., Chauville, J., & Letourneur, N. 1991, *A&A*, 245, 575
 Cassatella, A., Altamore, A., & González-Riestra, R. 2002, *A&A*, 384, 1023
 Cassatella, A., González-Riestra, R., & Selvelli, P. 2004, *INES Access Guide No.3 Classical Novae (ESA: Netherlands)*
 Chochol, D., Hric, L., & Papousek, J. 1981, *IBVS*, No. 2059
 Fernandez-Castro, T., González-Riestra, R., Cassatella, A., Taylor, A. R. & Seaquist, E. R. 1995, *ApJ*, 442, 366
 Friedjung, M., Ferrarri-Toniolo, M., Persi, P., Altamore, A., Cassatella, A., & Viotti, R. 1984 in *The Future of Ultraviolet Astronomy Based on Six Years of IUE Research*, NASA CP-2349, eds. J.M. Mead, R.D. Chapman, & Y. Kondo (NASA, Washington,DC) p.305
 Goehermann, J. 1991, *A&A*, 250, 361
 Grevesse, N. 2008, in *Comm. in Asteroseismology*, 157, 156
 Hachisu, I., & Kato, M. 2006, *ApJS*, 167, 59
 Hachisu, I., & Kato, M. 2010, *ApJ*, 709, 680
 Hachisu, I., Kato, M., & Cassatella, A. 2008, *ApJ*, 687, 1236
 Hachisu, I., Kato, M., & Nomoto, K. 1999a, *ApJ*, 522, 487
 Hachisu, I., Kato, M., Nomoto, K., & Umeda, H. 1999b, *ApJ*, 519, 314
 Hayashi, C., Hoshi, R., & Sugimoto, D. 1962, *progress of theoretical physics, supplement*, 22, 1
 Hoard, D.W., Wallerstein, G., & Willson, L.A. 1996, *PASP*, 108, 81
 Hric, L., Chochol, D., & Grygar, J. 1980, *IBVS*, No. 1835
 Iben, I., Jr. 1965, *ApJ*, 142, 1447
 Iben, I., Jr. 1982, *ApJ*, 259, 244
 Iijima, T. 1989, *A&A*, 215, 57
 Iijima, T., & Ortolani, S. 1984, *A&A*, 136, 1
 Iglesias, C. A., & Rogers, F. J. 1996, *ApJ*, 464, 943
 José, J., & Hernanz, M. 1998, *ApJ*, 494, 680
 Kanamitsu, O. 1991a, *PASJ*, 43, 225
 Kanamitsu, O., Yamashita, Y., Norimoto, Y., Watanabe, E., & Yutani, M. 1991b, *PASJ*, 43, 523
 Kato, M. 1985, *PASJ*, 37, 19
 Kato, M. 2010, *Astron. Hachr.(AN)*, 331, 140
 Kato, M., & Hachisu, I., 1994, *ApJ*, 437, 802
 Kato, M., & Hachisu, I., 2005, *ApJ*, 633, L117
 Kato, M., & Hachisu, I. 2007, *ApJ*, 657, 1004
 Kato, M., & Hachisu, I. 2009, *ApJ*, 699, 1293
 Kato, M., Hachisu, I., & Cassatella, A. 2009, *ApJ*, 704, 1676
 Kato, M. & Iben, Jr. I., 1992, *ApJ*, 394, 305
 Kenyon, S.J. 1986, *AJ*, 91, 563
 Klein, A., Bruch, A., & Luthardt, R. 1994, *A&AS*, 104, 99
 Kolotilov, E. A. 1983, *Soviet Astronomy*, 27, 432
 Kolotilov, E. A., Munari, U., & Yudin, B.F. 1995, *MNRAS*, 275, 185
 Kozai, Y. 1979a, *IAU Circ.*, No. 3344
 Kozai, Y. 1979b, *IAU Circ.*, No. 3348
 Liller, M., & Liller, W. 1979, *AJ*, 84, 1357
 Luna, G.J.M., & Costa, R.D.D. 2005, *A&A*, 435, 1087
 Mürset, U., Wolff, B., & Jordan, S. 1997, *A&A*, 319, 201
 Nariai, K., Nomoto, K., & Sugimoto, D. 1980, *PASJ*, 32, 473
 Nussbaumer, H., & Vogel, M. 1996, *A&A*, 307, 470
 Prialnik, D. 1986, *ApJ*, 310, 222
 Prialnik, D., & Kovetz, A. 1995, *ApJ*, 445, 789
 Purgathofer, A., & Schnell, A. 1982, *IBVS*, No. 2071
 Purgathofer, A., & Schnell, A. 1983, *IBVS*, No. 2264
 Seaton, M. J. 1979, *MNRAS*, 187, 73–76, *Interstellar extinction in the UV*
 Sion, E. M., Shore, S.N., Ready, C. J., Scheible, M. P. 1993, *AJ*, 106, 2118
 Skopal, A. 2006, *A&A*, 457, 1003
 Starrfield, S., Sparks, W. M., & Shaviv, G. 1988, *ApJ*, 325, L35

- Starrfield, S. Truran, J. W., Sparks, W. M., & Kutter, G. S. 1972, ApJ, 176, 169
- Tamura, S., Kanamitsu, O., & Yamashita, Y. 1992, PASJ, 44, 543
- Tomov, T., Zamanov, R., Iliev, L., Mikolajewski, M., & Georgiev, L. 1991, MNRAS, 252, 31
- Vogel, M., & Nussbaumer, H. 1992, A&A, 259, 525
- Wenzel, W. 1979, IBVS, No. 1608
- Yamashita, Y., Maehara, H., Norimoto, Y. 1982, PASJ, 34, 269
- Yamashita, Y., Norimoto, Y., & Yoo, K.H. 1983, PASJ, 35, 521
- Yoo, K-H. 2007, Journal of the Korean Astronomical Society, 40, 39
- Yoon, T.S., & Honeycutt, R.K. 2000, PASP, 112, 335